Journal of Materials Chemistry B

COMMUNICATION

View Article Online
View Journal | View Issue

Cite this: J. Mater. Chem. B, 2014, 2, 1121

Received 16th November 2013
Accepted 17th December 2013

DOI: 10.1039/c3tb21617a

www.rsc.org/MaterialsB

Template-free synthesis of uniform mesoporous SnO_2 nanospheres for efficient phosphopeptide enrichment†

Liping Li,‡[a] Shuai Chen,‡[b] Linnan Xu,[a] Yu Bai,*[a] Zongxiu Nie,[c] Huwei Liu[a] and Limin Qi*[b]

A one-step and template-free method to prepare uniform SnO_2 nanospheres with a mesoporous structure was developed for the applications in phosphopeptide enrichment. The as-synthesized mesoporous SnO_2 nanospheres have a large surface area and highly active surfaces for the effective binding of phosphopeptides. Compared with the non-porous SnO_2 and commercial TiO_2, mesoporous SnO_2 nanospheres represent superior performance in the specific trapping of phosphopeptides from both standard protein and complex nonfat milk digests for mass spectrometry-based phosphoproteomic analysis. The feasible synthetic approach and the excellent enrichment performance make the mesoporous SnO_2 nanospheres promising in further phosphoproteomic research.

Protein phosphorylation, one of the most common post-translational modifications, is of great importance in regulating various biological processes,[1] and powerful sample preparation methods for in-depth exploration of phosphorylation-related biological processes have long been in urgent demand.[2] Among those methods metal oxide affinity chromatography (MOAC) takes advantage of the excellent selectivity of various metal oxides, which leads to a rapid increase of its applications.[3] The basic mechanism of MOAC is based on the affinity between the phosphate group and metal oxides acting as Lewis acid under acidic conditions. The surface properties of different metal oxide nanomaterials affect their affinity towards phosphopeptides, which often leads to different enrichment performance[4] in sensitivity,[5] specificity[6–9] or phosphoproteome coverage.[10–12] Therefore, both the component and structure of nanomaterials are crucial in designing effective affinity probes.

Due to their large surface area with high surface activity and ready modification, mesoporous nanomaterials are considered promising in various fields[13–16] and have already attracted increasing attention for the development of an effective sample preparation method.[14–19] With relatively higher Lewis acidity, SnO_2 is considered as an ideal complement for the existing affinity probes and several SnO_2-based nanomaterials were prepared for the improvement of phosphoproteomic analysis.[4,5,20,21] Reports of other metal oxides demonstrated that mesoporous structures have great potential for efficient phosphopeptide enrichment.[10,11,17] Therefore, mesoporous SnO_2 nanospheres for biological application and their detailed performance are well worth being investigated. Several literature studies reported the synthesis of mesoporous SnO_2 spheres as well as their applications in gas sensing, lithium-ion batteries, and photocatalysis.[22–27] However, the synthesis was mostly carried out with the assistance of organic additives or templates,[22,23,26–29] which may result in complex steps in synthesis or uncontrollable interferents in phosphopeptide binding and thus limits their practical applications. On the other hand, mesoporous SnO_2 nanospheres with sizes less than 100 nm have been prepared without organic additives, but their surface areas were generally not very high and the application of mesoporous SnO_2 nanospheres in MOAC materials has not been well explored so far.[24,25,30] Hence, it is well worth putting more effort into developing template-free and simple synthetic methods to obtain mesoporous SnO_2 nanospheres with high surface areas and ideal surface properties for large-scale phosphoproteomic analysis.

Herein we report the facile synthesis of nearly monodisperse mesoporous SnO_2 nanospheres *via* a one-step, template-free solvothermal method for efficient phosphopeptide enrichment. First, owing to the mesoporous structure, these uniform SnO_2 nanospheres have a large surface area of 109.9 $m^2\ g^{-1}$, which results in more active sites exposed for the effective binding of

[a]Beijing National Laboratory for Molecular Sciences, Key Laboratory of Bioorganic Chemistry and Molecular Engineering of Ministry of Education, College of Chemistry, Peking University, Beijing 100871, China. E-mail: yu.bai@pku.edu.cn; Tel: +86 10 6275 8198

[b]Beijing National Laboratory for Molecular Sciences, State Key Laboratory for Structural Chemistry of Stable and Unstable Species, College of Chemistry, Peking University, Beijing 100871, China. E-mail: liminqi@pku.edu.cn

[c]Key Laboratory of Analytical Chemistry for Living Biosystems, Institute of Chemistry, The Chinese Academy of Sciences, Beijing 100190, China

† Electronic supplementary information (ESI) available. Experimental procedures, characterization of materials, detected phosphopeptides and their sequences. See DOI: 10.1039/c3tb21617a

‡ These authors contributed equally to the work.

phosphopeptides. Second, the absence of organic additives, such as surfactants, reduces uncontrollable interferents, which makes the mesopores accessible during the binding step of the phosphopeptide enrichment. Third, the simplicity of this synthesis makes it feasible for biological applications and nanomaterials commercialization. The subsequent MS-based phosphoproteomics analysis showed excellent performance in both sensitivity and real sample analysis by using these mesoporous SnO_2 nanospheres, indicating their promising potential in phosphoproteomic research.

Mesoporous SnO_2 nanospheres were synthesized by a facile solvothermal treatment of the solution consisting of ethanol, hydrochloride acid and $SnCl_4 \cdot 5H_2O$. Fig. 1a shows a low-magnification SEM image of the obtained nanospheres after the solvothermal reaction at 150 °C for 24 h, which suggests the large-scale formation of nearly monodisperse nanospheres with an average diameter of ~70 nm. The high-magnification SEM image shows that all the nanospheres have a rough surface, indicating that each nanosphere consists of primary nanoparticles (Fig. 1b). The TEM image shown in Fig. 1c reveals the mesoporous structure of a typical nanosphere consisting of nanoparticles of about 5 nm in size. The related selected-area electron diffraction (SAED) pattern shows clearly rings characteristic of rutile SnO_2. The HRTEM image shown in Fig. 1d exhibits clear lattice fringes with d spacings of 0.34 nm and 0.26 nm, which can be indexed to the (110) and (101) plane of rutile SnO_2, respectively. The X-ray diffraction (XRD) pattern shown in Fig. 1e reveals that all the diffraction peaks can be ascribed to SnO_2 crystals with a tetragonal rutile phase (JCPDS no. 41-1445), which is consistent with the SAED results. Detailed analysis of the peak broadening of the (101) reflection using the Scherrer equation indicates an average crystalline size of 5.3 nm, which is in agreement with the TEM results. The N_2 adsorption–desorption isotherm shows a type-IV isotherm with a hysteresis loop in the relative pressure range (P/P_0) of 0.8–1.0 (Fig. 1f), which suggests a mesoporous structure. An average pore size of around 12 nm was calculated from the desorption branch of the nitrogen sorption isotherm using the BJH (Barrett–Joyner–Halenda) model. The mesoporous SnO_2 nanospheres have a BET (Brunauer–Emmett–Teller) surface area of 109.9 $m^2\ g^{-1}$, which is very high for SnO_2 considering its high density (6.95 $g\ cm^{-3}$). This surface area is considerably higher than those of the reported mesoporous SnO_2 nanospheres with similar sizes synthesized without organic additives.[24,25,30]

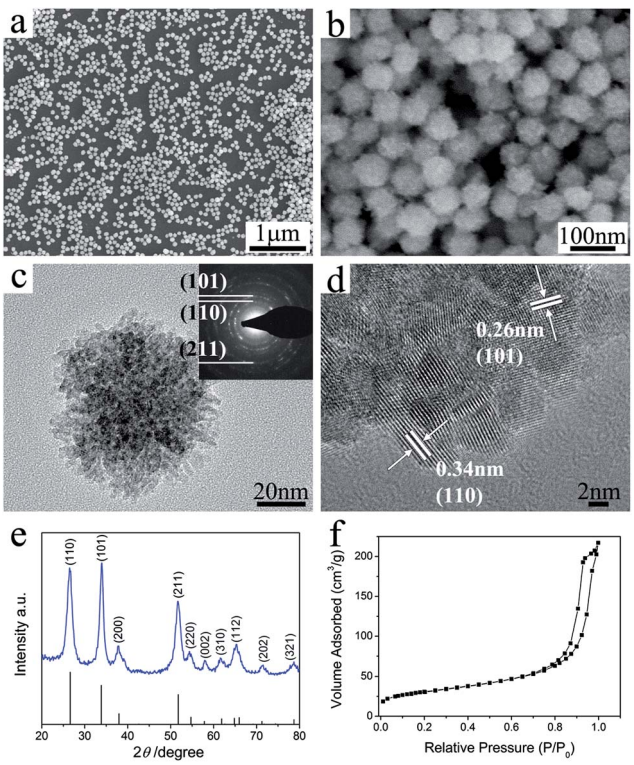

Fig. 1 SEM images (a and b), TEM image (c), HRTEM image (d), XRD pattern (e) and N_2 adsorption–desorption isotherm (f) of mesoporous SnO_2 nanospheres. The inset in (c) is the corresponding SAED pattern.

It was found that hydrochloride acid has binary effects on controlling the hydrolysis process in this ethanol solvent system. A synthesis system comprising 50 μL of concentrated aqueous HCl in 8 mL ethanol is adopted after optimization. Firstly, hydrochloride acid afforded water for the hydrolysis of $SnCl_4$. When no hydrochloride acid was added, the hydrolysis process of Sn^{4+} was greatly inhibited, resulting in a very low output of smaller porous nanospheres (Fig. 2a). The hydrolysis process could still occur without hydrochloride acid due to the small amount of water in $SnCl_4 \cdot 5H_2O$ and ethanol. Secondly, hydrochloride acid acted as a proton donor to control the hydrolysis rate of Sn^{4+}. Fig. 2b shows the products obtained with addition of 50 μL water instead of HCl solution. The yield of products was increased, but the uneven size of products reveals that the hydrolysis rate was not well controlled without the acidity of HCl. If the amount of concentrated hydrochloride acid was increased from 50 μL to 200 μL, the hydrolysis rate was too fast, and irregular aggregates of small nanoparticles were obtained (Fig. 2c), indicating that an appropriate amount of hydrochloride acid is the key to keep a moderate hydrolysis rate.

This mesoporous SnO_2 synthetic method has several advantages for the applications of mesoporous SnO_2 nanospheres in phosphopeptide enrichment: (1) by this facile route, uniform mesoporous SnO_2 nanospheres can be achieved without templates or organic additives, which eliminates interferents and makes the active surface of the material fully accessible to the peptides; (2) with the mesoporous structure and relatively high density, the mesoporous SnO_2 nanospheres provide a highly active binding surface as well as convenient

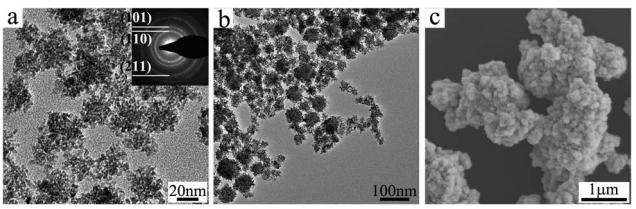

Fig. 2 TEM (a and b) and SEM (c) images of SnO_2 products obtained with addition of different amounts of hydrochloride acid or water: (a) without addition of hydrochloride acid and water, (b) 50 μL water, (c) 200 μL concentrated hydrochloride acid.

downstream separation by using usual centriguation; (3) this facile synthesis approach is cost efficient, environmentally friendly, and easy to be scaled up for widespread applications in phosphoproteomic analysis.

As illustrated in Fig. 3a, phosphopeptide enrichment from the tryptic protein digests was performed in a batch mode using the as-synthesized mesoporous SnO_2 ($mSnO_2$) nanospheres as the affinity probe. MALDI-ToF mass spectra show the tryptic digested β-casein (4×10^{-7} M) before and after enrichment by mesoporous SnO_2. Three phosphopeptides were detected with the highest signal to noise ratio (S/N) of 4821 in the digests of β-casein (4×10^{-7} M) with enrichment by using mesoporous SnO_2 (Fig. 3c), which demonstrated the strong affinity of mesoporous SnO_2 towards phosphopeptides. Under the same conditions, both SnO_2 nanoparticles with a smaller surface area of 39.9 $m^2\ g^{-1}$ (shown in Fig. S1 and S2†) and commercial TiO_2 showed similar results (Fig. S3†). However, mesoporous SnO_2 revealed much better enrichment efficiency when the concentration of β-casein was lowered to 4×10^{-10} M (Fig. 4). Under such low concentration, only one phosphopeptide was detected after enrichment by either non-porous SnO_2 nanoparticles or commercial TiO_2, while three ones were detected after enrichment by mesoporous SnO_2. This result indicated a more effective and accurate detection of β-casein under low concentration by $mSnO_2$, which was superior to previous reports using non-porous SnO_2 as affinity probes,[5,20] highlighting the relatively higher sensitivity of mesoporous

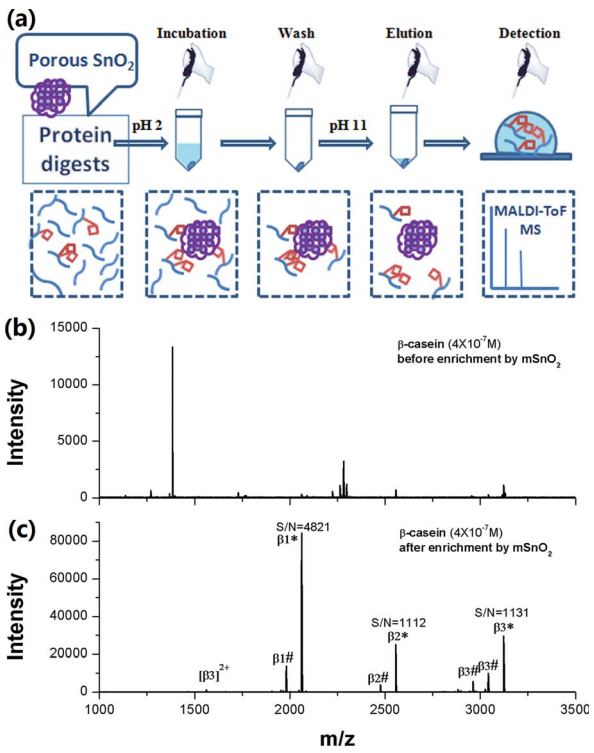

Fig. 3 Scheme of phosphopeptide enrichment (a) and MALDI-ToF mass spectra of tryptic digested β-casein (4×10^{-7} M) without enrichment (b) and after enrichment by mesoporous SnO_2 (c). (* phosphopeptides and # peptide residues from phosphoric acid neutral loss of phosphopeptides).

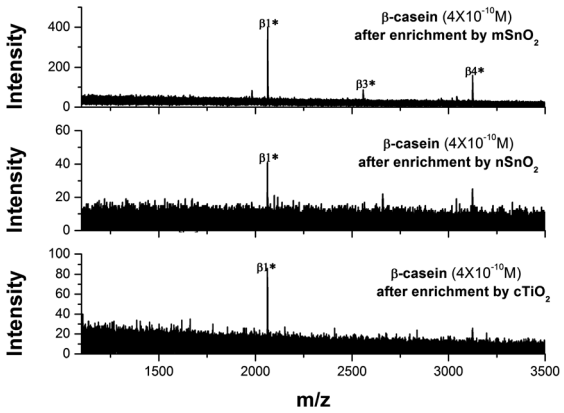

Fig. 4 Phosphopeptide enrichment from β-casein (4×10^{-10} M) by using $mSnO_2$, $nSnO_2$ and $cTiO_2$ (* phosphopeptides, $mSnO_2$: mesoporous SnO_2, $nSnO_2$: non-porous SnO_2, $cTiO_2$: commercial TiO_2).

SnO_2 generated from their highly accessible active surfaces and large binding area. It is interesting that researchers have proved that the rutile form of titania exhibited better selectivity for the phosphopeptide,[31] and the same phenomenon has been found for our synthesized rutile SnO_2. All these features are promising in actual applications considering the high dynamic range of phosphoproteins in biological samples.

To demonstrate their ability to improve phosphoproteomic analysis in complex real samples, these mesoporous nanospheres were further tried to trap phosphopeptides in protein digests from nonfat milk. Before enrichment most of the detected peaks corresponded to nonphosphorylated peptides (Fig. S4†), while the signals of phosphorylated ones dominated the MS spectrum after treatment by mesoporous SnO_2, as shown in Fig. 5. These mesoporous materials also revealed higher efficiency from the comparison of the MS results of SnO_2 nanoparticles and commercial TiO_2. Using the same nonfat milk digests, 10 phosphopeptides were detected by SnO_2 nanoparticles or commercial TiO_2, while 17 phosphopeptides were detected after enrichment by mesoporous SnO_2. The detailed information of the detected phosphopeptides is listed in Table S1.† This result demonstrated that the large surface

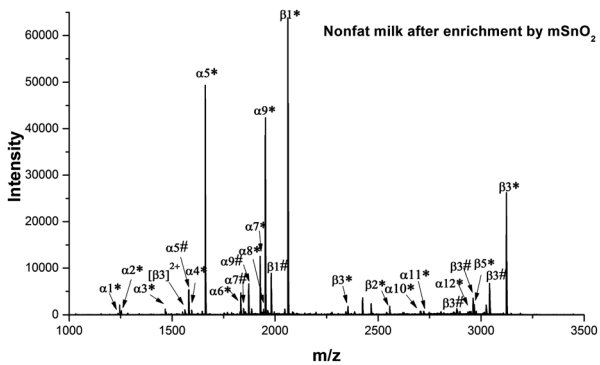

Fig. 5 MALDI-ToF mass spectrum of tryptic digested diluted nonfat milk after enrichment by mesoporous SnO_2 (* phosphopeptides and # peptide residues from phosphoric acid neutral loss of phosphopeptides).

area, highly active binding sites and fully accessible surfaces of these SnO_2 spheres are beneficial for binding equilibrium and thus strengthen the enrichment efficiency from complex samples. Meanwhile, high-quality SnO_2 nanospheres with all the above advantages were obtained by a feasible synthetic method, thus it was practical for the full utilization of their advantages in further phosphoproteomic research on more complex biological systems.

In summary, a feasible synthetic approach for preparation of highly uniform mesoporous SnO_2 nanospheres *via* a template-free solvothermal method was developed. The absence of templates during synthesis helped to generate an accessible binding surface, and the resulting SnO_2 nanospheres have a mesoporous structure and a relatively high density, which offer a large surface area together with convenience in centrifugal separation. In addition, the synthesis was cost efficient, environmentally friendly and easy to be amplified for large scale applications. All the above advantages made the mesoporous SnO_2 nanospheres promising MOAC affinity probes with high sensitivity in both laboratory and real systems. We believe this work is the starting point for investigating applications of mesoporous SnO_2 in phosphopeptide enrichment and detection, and more complex biological samples are well-worth exploring in further study, especially in phosphoproteomic study. Furthermore, our work indicates that developing feasible methods for the synthesis of high-quality metal oxides should be considered in the screening of efficient and applicable MOAC affinity probes in target proteomic research.

Acknowledgements

The authors gratefully acknowledge the National Natural Science Foundation of China (no. 21322505, 21175008, 21073005, and 51121091) and Special-funded Programme on Innovative Approaches, Ministry of Science and Technology of China (no. 2012IM030900) for the funding support.

Notes and references

1 D. F. Stern, *Exp. Mol. Pathol.*, 2001, **70**, 327–331.
2 A. Leitner, M. Sturm and W. Lindner, *Anal. Chim. Acta*, 2011, **703**, 19–30.
3 A. Leitner, *TrAC, Trends Anal. Chem.*, 2010, **29**, 177–185.
4 M. Sturm, A. Leitner, J.-H. Smatt, M. Linden and W. Lindner, *Adv. Funct. Mater.*, 2008, **18**, 2381–2389.
5 D. W. Qi, J. Lu, C. H. Deng and X. M. Zhang, *J. Phys. Chem. C*, 2009, **113**, 15854–15861.
6 S. B. Ficarro, J. R. Parikh, N. C. Blank and J. A. Marto, *Anal. Chem.*, 2008, **80**, 4606–4613.
7 D. W. Qi, J. Lu, C. H. Deng and X. M. Zhang, *J. Chromatogr., A*, 2009, **1216**, 5533–5539.
8 J. Yan, X. Li, S. Cheng, Y. Ke and X. Liang, *Chem. Commun.*, 2009, 2929–2931.
9 L. P. Li, T. Zheng, L. N. Xu, Z. Li, L. D. Sun, Z. X. Nie, Y. Bai and H. W. Liu, *Chem. Commun.*, 2013, **49**, 1762–1764.
10 C. A. Nelson, J. R. Szczech, C. J. Dooley, Q. G. Xu, M. J. Lawrence, H. Y. Zhu, S. Jin and Y. Ge, *Anal. Chem.*, 2010, **82**, 7193–7201.
11 J. Tang, P. Yin, X. H. Lu, D. W. Qi, Y. Mao, C. H. Deng, P. Y. Yang and X. M. Zhang, *J. Chromatogr., A*, 2010, **1217**, 2197–2205.
12 A. Leitner, M. Sturm, O. Hudecz, M. Mazanek, J. H. Smatt, M. Linden, W. Lindner and K. Mechtler, *Anal. Chem.*, 2010, **82**, 2726–2733.
13 A. Corma, *Chem. Rev.*, 1997, **97**, 2373–2419.
14 B. J. Scott, G. Wirnsberger and G. D. Stucky, *Chem. Mater.*, 2001, **13**, 3140–3150.
15 M. Hartmann, *Chem. Mater.*, 2005, **17**, 4577–4593.
16 L. Zhao, H. Qin, R. A. Wu and H. Zou, *J. Chromatogr., A*, 2012, **1228**, 193–204.
17 Z. D. Lu, J. C. Duan, L. He, Y. X. Hu and Y. D. Yin, *Anal. Chem.*, 2010, **82**, 7249–7258.
18 C. A. Nelson, J. R. Szczech, Q. Xu, M. J. Lawrence, S. Jin and Y. Ge, *Chem. Commun.*, 2009, 6607–6609.
19 W. F. Ma, Y. Zhang, L. L. Li, L. J. You, P. Zhang, Y. T. Zhang, J. M. Li, M. Yu, J. Guo, H. J. Lu and C. C. Wang, *ACS Nano*, 2012, **6**, 3179–3188.
20 J. Lu, D. W. Qi, C. H. Deng, X. M. Zhang and P. Y. Yang, *Nanoscale*, 2010, **2**, 1892–1900.
21 R. N. Ma, J. J. Hu, Z. W. Cai and H. X. Ju, *Talanta*, 2014, **119**, 452–457.
22 H. Wang, J. Xu and Q. Pan, *CrystEngComm*, 2010, **12**, 1280–1285.
23 P. M. R. Boppella and S. V. Manorama, *ACS Appl. Mater. Interfaces*, 2012, **4**, 6252–6260.
24 Z. Miao, Y. Wu, X. Zhang, Z. Liu, B. Han, K. Ding and G. An, *J. Mater. Chem.*, 2007, **17**, 1791–1796.
25 Z. Li, Q. Zhao, W. Fan and J. Zhan, *Nanoscale*, 2011, **3**, 1646–1652.
26 R. Demir-Cakan, Y. S. Hu, M. Antonietti, J. Maier and M. M. Titirici, *Chem. Mater.*, 2008, **20**, 1227–1229.
27 Y. Chen, J. Ma, L. Yu, Q. Li and T. Wang, *CrystEngComm*, 2012, **14**, 6170–6172.
28 S. K. Tripathy, A. Mishra, S. K. Jha, R. Wahab and A. A. Al-Khedhairy, *J. Mater. Sci.: Mater. Electron.*, 2013, **24**, 2082–2090.
29 B. Jia, W. Jia, F. Qu and X. Wu, *RSC Adv.*, 2013, **3**, 12140–12148.
30 H. Zhang, Q. He, X. Zhu, D. Pan, X. Deng and Z. Jiao, *CrystEngComm*, 2012, **14**, 3169–3176.
31 K. Imami, N. Sugiyama, Y. Kyono, M. Tomita and Y. Ishirama, *Anal. Sci.*, 2008, **24**, 161–166.

